Available online at www.sciencedirect.com
SCIENCE DIRECT
Journal of volcanology and geothermal research
Journal of Volcanology and Geothermal Research 154 (2006) 303–316
www.elsevier.com/locate/jvolgeores

BND (bubble number density) decompression rate meter for explosive volcanic eruptions

A. Toramaru *

Department of Earth and Planetary Sciences, Kyushu University, Higashiku, 6-10-1 Hakozaki, Fukuoka 812-8581, Japan

Received 8 September 2004; received in revised form 13 March 2006; accepted 20 March 2006
Available online 12 May 2006

Abstract

This decade has been witness to substantial progress in the understanding of bubble dynamics and its role in volcanic eruptions. A comparison between the results of experiments and a model for bubble nucleation shows that bubble number density (BND) can be calculated as a function of decompression rate for given physical properties, such as the diffusivity of water in a silicate melt and interfacial tension, within an acceptable margin of error. Conversely, in this paper, we propose a method (hereafter referred to as BND decompression rate meter) to estimate the decompression rate by using BND data of natural pumice samples from volcanic eruptions. As a result of the application of the BND decompression rate meter to pumice and scoria from explosive eruptions, it is found that the decompression rates increase in the range from 10^6 to 10^8 (Pa/s) with the eruption column heights; these rates are proportional to the 4th power of the eruption column heights and are linear to the discharge rates. The absolute values of the estimated decompression rates are very high and cannot be explained by the existing models of conduit flows. In order to explain such high rates of decompression and the correlation with discharge rate, we propose a possible model according to which the bubble nucleation propagates downward as a rarefaction shock wave in the conduit.

Keywords: bubble number density; pumice; scoria; decompression rate; explosive eruption; quantification of eruption; column height

1. Introduction

Although there exits a number of studies (Mader et al., 1997; Sparks, 1978; Jaupart and Allègre, 1991; Hurwitz and Navon, 1994; Woods, 1995; Proussevitch and Sahagian, 1996) related to the dynamics of volcanic eruption, a quantitative understanding of the dynamics, such as decompression and water exsolution rates in the conduit, during eruption is still poor from the observational and material-scientific points of view. This is primarily due to our inability to directly measure the physical condition in the interior of the conduit during eruptions. Hence, we need to devise a method to quantify the intra-conduit processes during eruption, which will facilitate a new understanding of the eruption dynamics. Pyroclasts, such as pumice or scoria, that are produced by explosive eruptions possibly record the physical state in the conduit during eruptions (Toramaru, 1989, 1990; Gardner et al., 1996). In particular, bubbles in pyroclasts are fossils of magma vesiculation, which is the driving force behind explosive eruptions. Hence, the examination of bubbles in pyroclasts can be developed as a tool for the quantifcation of intra-conduit processes during eruptions.

* Tel.: +81 92 642 2648; fax: +81 92 642 2684.
E-mail address: toramaru@geo.kyushu-u.ac.jp.

0377-0273/$ - see front matter © 2006 Elsevier B.V. All rights reserved.
doi:10.1016/j.jvolgeores.2006.03.027

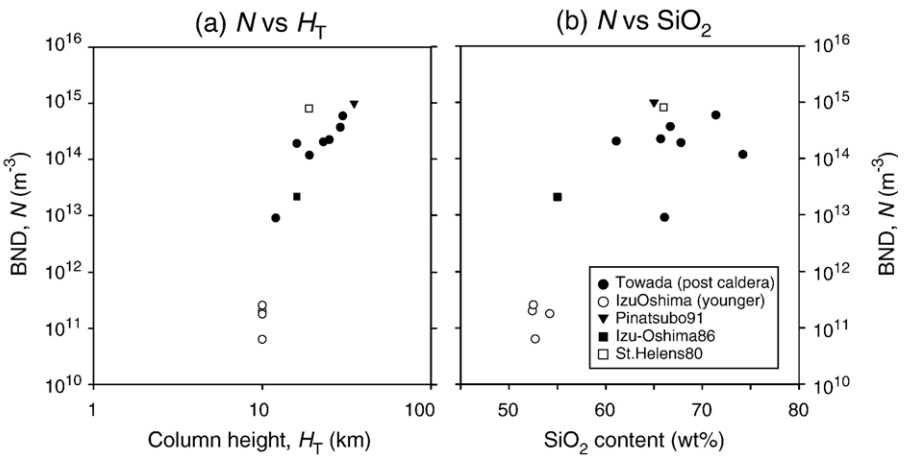

Fig. 1. (a) BNDs vs. eruption column heights and (b) BNDs vs. SiO_2 content of bulk rock for 14 Plinian eruptions (Towada: solid circle, Izu-Oshima: open circle, Pinatubo 1991: solid triangle, Izu-Oshima, 1986 solid square, St. Helens 1983: open square). See Table 1 for the details.

Fig. 1 shows the correlations of the bubble number density (BND) in pumices with (a) column heights and (b) SiO_2 content. BND data obtained from the textural analysis of pumice and scoria in Plinian to subplinian type eruptions in Japan (Towada and Izu-Oshima volcanoes) (Toramaru, 1990, 1995) Izu-Oshima 1986 eruption (Miwa and Toramaru, in preparation), Mount Pinatubo 1991 eruption (Polacci et al., 2001) and Mount St. Helens 1980 eruption (Klug and Cashman, 1994) are plotted (see also Table 1). Fig. 1(a) shows that the BND is a possible indicator of the physical processes in the conduit because the column height is controlled by the intra-conduit processes (e.g., Wilson et al., 1978). In addition, recent experimental (Mangan and Sisson, 2000; Mourtada-Bonnefoi and Laporte, 2002, 2004, Mangan et al., 2004; Gardner and Denis, 2004) (Fig. 2) numerical (Toramaru, 1995), and analytical (Yamada et al., 2005) studies show that BND strongly depends on

Table 1

Eruption	SiO_2 (wt.%)	Column height (km)	BND (m^{-3})	Microlite texture	Estimated decompression rate (Pa s^{-1})	Form of BSD
Towada-A[a]	71.4	30	6.0×10^{14}	Very sparse	6.4×10^{7}	Exponential
Towada-B[a]	74.2	19	1.2×10^{14}	Very sparse	1.8×10^{7}	Not determined
Towada-C[a]	66.7	329	3.7×10^{14}	Very sparse	7.0×10^{7}	Exponential
Towada-D[l]	67.8	16	1.9×10^{14}	Very sparse	4.1×10^{7}	Exponential
Towada-E[a]	65.7	25	2.2×10^{14}	Very sparse	5.6×10^{7}	Inconclusive
Towada-F[a]	61.1	23	2.0×10^{14}	Abundant	9.1×10^{7}	Inconclusive
Towada-G[a]	66.1	12	9.0×10^{12}	Very sparse	6.3×10^{6}	Exponential
Izu-Oshima-Y1[a]	52.4	10	2.0×10^{11}	Moderate	3.4×10^{6}	Power law
Izu-Oshima-Y2[a]	52.7	10	6.4×10^{10}	Moderate	1.5×10^{6}	Exponential
Izu-Oshima-Y5[a]	54.2	10	1.8×10^{11}	Unknown	2.3×10^{6}	Power law
Izu-Oshima-Y6[a]	52.5	10	2.6×10^{11}	Abundant	4.0×10^{6}	Power law
Pinatsubo 1991[b]	65.0	35	1.0×10^{15}	Very sparse	1.6×10^{8}	Normal
Izu-Oshima 1986B[c]	55.0	16	2.1×10^{13}	Abundant	4.9×10^{7}	Power law
St Helens 1980[d]	66.0	19	8.2×10^{15}	Very sparse	1.4×10^{8}	Log-normal

[a] Historical eruptions of Towada and Izu-Oshima volcanoes: BNDs are value given in Toramaru (1995). Microlite textures are based on the observation by the SEM and optical microscope. Form of BSD (Bubble Size Distribution) is from Blower et al. (2002).

[b] Pinatubo 1991: BND is a representative value calculated by $BND=N_A/d$ for the groundmass of white pumice from the data by Polacci et al. (2001) where N_A is a number density per unit area and d is an average bubble size. Microlite texture is based on Table 3 of Polacci et al. (2001).

[c] Izu-Oshima 1986B: BND, microlite texture, and form of BSD are based on the observation by the SEM and optical microscope (Miwa and Toramaru, in preparation).

[d] St Helens 1980: BND, microlite texture, and form of BSD are the data for white pumice from Table 1 by Klug and Cashman (1994).

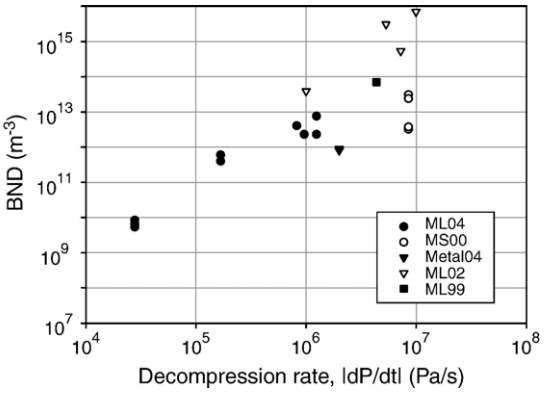

Fig. 2. Compiled experimental data of the BND as a function of the decompression rate. In the legend, ML04 refers to data from Mourtada-Bonnefoi and Laporte (2004): MS00, Mangan and Sisson (2000); Metal104, Mangan et al. (2004), ML02, Mourtada-Bonnefoi and Laporte (2002) and ML99 Mourtada-Bonnefoi and Laporte (1999). In this plot, experiments (Gardner et al., 1999, 2000; Larsen and Gardner, 2004; Gardner and Denis, 2004) that were characterized by the occurrence of a heterogeneous nucleation of bubbles are excluded. Furthermore, data that were obtained from experiments by Mangan and Sisson (2000) with a lower decompression rate, are not plotted due to the influence of the nucleation and growth of bubbles on the capsule wall (Mangan, personal communication).

the decompression rate. On the other hand Fig. 1(b) implies that the BND is controlled by physical properties, such as diffusivity, viscosity, and interfacial energy, through their SiO_2 content dependence. Hence, in order to discriminate between these two possibilities for the BND variations, we need to accurately evaluate the effects of both the physical process (or decompression rate) and the physical properties. In other words, this evaluation can be made possible by developing a methodology to accurately estimate the decompression rate from the BND data.

In this paper, on the basis of the abovementioned background, we devise a tool to estimate the decompression rate from the BND data (hereafter referred to as BND decompression rate meter). First, we introduce a procedure to construct the BND decompression rate meter by presenting appropriate expressions of physical properties such as diffusivity of H_2O in melts. Second, for the BND decompression rate meter, we illustrate the effect of SiO_2 and H_2O contents on the estimated decompression rate. Third, we apply the BND decompression rate meter to the reported BND data and correlate it with the eruption column heights and discharge rates. Finally, we discuss the estimated values of the decompression rates and their correlation with the discharge rates and propose a new concept for the bubble nucleation process in the conduit in order to explain the values of the estimated decompression rates.

2. Construction of the BND decompression rate meter

Recently, Mourtada-Bonnefoi and Laporte (2004) showed that the bubble number density (BND) data obtained from decompression experiments performed on a rhyolitic melt can be satisfactorily explained by a numerical model, (Toramaru, 1995). In both the experiments and model, a single event of homogeneous nucleation of bubbles occurs under constant rates of decompression; hence, we must deal with pyroclasts that preserve the BND determined by the event. The model predicts that the BND is a function of the decompression rate and physical properties, such as the diffusivity of water in a silicate melt and interfacial tension by the following empirical relationship

$$N = 34 \cdot C \cdot \alpha_1^{-2} \cdot \alpha_2^{-1/4} \cdot \alpha_3^{-3/2} \quad (1)$$

where N is the BND (m^{-3}); C, the initial water concentration in molecular number per cubic meters (number m^{-3}); and the factor 34, a value determined by the parameter study in the numerical study (Toramaru, 1995). α_1 α_2, and α_3 are dimensionless parameters that control the solutions in the model. They are defined as $\alpha_1 = 16\pi\sigma^3/(3kTP_W^2)$, $\alpha_2 = V_m P_W/(kT)$, and $\alpha_3 = P_W^2 kTCD/(4\sigma^2)|dP/dt|^{-1}$, where σ is the supercritical water fluid/silicate melt interfacial tension (N/m); k the Boltzmann constant ($=1.38\times10^{-23}$ (J/K)); T, the temperature; P_W, the initial saturation pressure (Pa) related to an initial concentration C by the solubility relation (Burnham, 1975; V_m, the volume of a water molecule in a silicate melt ($=3\times10^{-29}$ (m^3) based on Toramaru (1989) further, note a typo in Toramaru (1995) wherein this value was given as 3×10^{-28}); D, the diffusivity of water in a silicate melt (m^2/s); and $|dP/dt|$, the absolute value of the decompression rate (Pa/s). Physically, α_1 α_2 and α_3 are the difficulty in nucleation, scaled initial saturation pressure, and ratio of the decompression time scale to the diffusion time scale, respectively (see Toramaru (1989, 1995)) for details).

In Eq. (1), we use the solubility relation $C=4.0\times10^{23} P_W^{1/2}$, substitute the constants and the three controlling parameters, and rearrange the equation as follows:

$$\left|\frac{dP}{dt}\right| = a_0 \cdot D \cdot \sigma^2 \cdot P_W^{-1/3} \cdot T^{-1/2} \cdot N^{2/3} \quad (2)$$

where a_0 is a constant ($a_0=3.5\times10^{14}$).

Recent experimental works have enabled accurate predictions of physical properties such as diffusivity D (m^2/s) and interfacial tension σ (N/m) as functions of temperature T (K) and initial saturation pressure P_W (Pa) or initial H_2O concentration C_W (wt.%) and SiO_2 content

C_S (wt.%). Interfacial tension σ can be expressed according to Bagdassarov et al. (2000) as

$$\sigma = 0.2366 \exp\left(-0.35 \times 10^{-6} \cdot P_W - 11 \times 10^3 \left(\frac{1}{T} - \frac{1}{1273}\right)/R\right) \quad (3)$$

where R is a gas constant, 8.3 (J/K). Details of the effect of H_2O content are provided in the discussion section.

In Eq. (14) in Zhang and Behrens (2000) the diffusivity D_{ZB2000} is given as a function of temperature, pressure, and H_2O content, but not the SiO_2 content. However, in order to represent the diffusivity of H_2O in melts more accurately, we have to devise an expression for the same as a function of temperature, pressure, H_2O content, as well as SiO_2 content.

$$D_{ZB2000}(C_W, T, P) = X \cdot \exp(m) \cdot \left\{1 + \exp\left[56 + m + X \cdot \left(-34.1 + \frac{44620}{T} + \frac{57.3(P \times 10^{-6})}{T}\right) - \sqrt{X} \cdot \left(0.091 + \frac{4.77 \times 10^6}{T^2}\right)\right]\right\} \quad (4-1)$$

where

$$m = -20.79 - \frac{5030}{T} - \frac{1.4(P \times 10^{-6})}{T} \quad (4-2)$$

and X is the mole fraction of the water in the melt on a single oxygen basis. P denotes the pressure that is equal to the pressure at the nucleation climax (i.e., nucleation pressure) P_n, and in general is not equal to the initial saturation pressure. Although the nucleation pressure can be estimated from C and σ, the procedure is complicated. The effect of pressure on diffusivity is negligibly small; hence, we can assume that $P = P_n = P_W$. The relationships between X, P_W, and C_W are given by

$$P = 20000 \times 10^6 X^2 \quad (4-3)$$

and

$$X = 0.0167 C_W. \quad (4-4)$$

In Eq. (4-3), the factor $20\,000 \times 10^6$ is obtained from $200 \times 10^6/(0.5/5)^2$ since the water solubility at 200 MPa is 0.5 mole fraction (single albite basis) of H_2O (Burnham, 1975). A factor of five is used to transform the mole fraction from the albite basis to the single oxygen basis, which is determined such that the diffusivity of water described in Eq. (6) is the same as that shown in Fig. 9(a) of Zhang and Behrens (2000) at 850 °C and 200 MPa. This value of this factor does not affect the solubility relation: $P_W = 200 \times 10^6/6.0^2 \times C_W^2 = 5.6 \times 10^6 \times C_W^2$. This equation can be transformed into the solubility relation $C = 4 \times 10^{23} \times P_W^{1/2}$ in terms of molecular number concentration C using $C_W = C/\rho \times (0.018/6 \times 10^{23}) \times 100$, where ρ is the density of the melt, assumed to be 2500 kg/m^3). In Eq. (4-4), the factor 0.0167 is obtained from $0.5/(6.0 \times 5)$ since a 0.5 mole fraction (single albite basis) of H_2O corresponds to 6.0 wt.%.

On the other hand, in Behrens et al. (2004), the diffusivity $D_{BZX2004}$ is given as a function of temperature T, saturation pressure P, and SiO_2 content C_S for 1 wt.% H_2O content.

$$D_{BZX2004}(P, T, C_S) = 10^{(-0.757 - 0.0868 C_S) + \frac{-14785 + 131.7 C_S}{T} + \frac{(3.079 - 0.049 C_S)(P \times 10^{-6})}{T}} \quad (5)$$

Combining Eqs. (4-1)–(4-4) and (5), we can use the following expression for diffusivity as a function of temperature, pressure, SiO_2 content C_S, and H_2O content C_W:

$$D(P(C_W), T, C_S) = D_{BZX2004}(P(C_W), T, C_S) \cdot \frac{D_{ZB2000}(C_W, T, P(C_W))}{D_{ZB2000}(1\ \text{wt.\%}, T, P(C_W))} \quad (6)$$

Fig. 3 shows a comparison of diffusivity expressions (4-1)–(4-4), (5), and (6), assuming a relationship between the temperature and SiO_2 content as later introduced. Thus, the right-hand side of Eq. (2) is now a function of (P_W, T, N) or (C_W, T, N,).

Using these formulae for diffusivity and interfacial energy, we can verify the agreement between the experimental $|dP/dt|$ and estimated $|dP/dt|$ Eq. (2) with Eqs. (3), (4-1)–(4-4), (5), and (6). The estimated values of $|dP/dt|$ systematically provide values of decompression rates that are three times smaller than the actual values for laboratory experiments (Mourtada-Bonnefoi and Laporte, 2002, 2004; Mastin et al., 2004. In order to best fit the estimated decompression rates to the experimental values, the factor in Eq. (2) must be $3.0 \times a_0$ ($=1.0 \times 10^{15}$). Hereafter, we use this value as a ($=3 \times a_0$). In addition, for experiments that consider the CO_2 effect (Mourtada-Bonnefoi and Laporte, 2002), the employed σ values (Eq. (2)) are reduced by half. Fig. 4 shows a comparison between the experimental and calculated values of $|dP/dt|$. In this figure, experiments by Gardner et al. (1999), Gardner et al. (2000), Gardner and Denis (2004), and Larsen and Gardner (2004), in which a heterogeneous nucleation evidently occurred, are not plotted. Some data by Mangan and Sisson (2000) do not agree with this model. This is probably due to the influence of the nucleation and growth of bubbles on the capsule wall in the experiments that employed a lower decompression

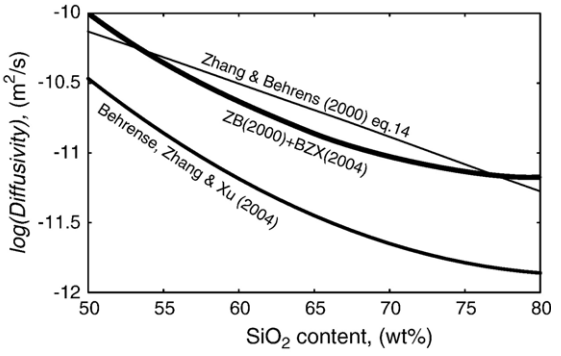

Fig. 3. Comparison of diffusivities as a function of SiO_2 content. The line with "Zhang and Behrens (2000) Eq. (14)" represents Eqs. (4-1)–(4-4). The curves with "Behrens, Zhang, and Xu (2004)" and with "ZB (2000)+BZT (2004)" represent Eqs. (5) and (6), respectively. The water saturation pressure of 100 MPa is assumed.

rate (Mangan, personal communication). Therefore, we have not plotted the data obtained under a lower decompression rate.

In general, the temperature of magma T is related to the SiO_2 content of the magma C_S. A simple empirical relationship (Toramaru, 1995) between T (K) and C_S (wt.%) is

$$T = \frac{1000}{0.16 + 0.001 C_S}. \tag{7}$$

This relationship was determined to approximate temperatures and SiO_2 contents of 20 lavas from 11 volcanoes. Finally, Eq. (2) defines the function of H_2O and SiO_2 contents and BND or N:

$$\left|\frac{dP}{dt}\right| = a \cdot D \cdot \sigma^2 \cdot P_W^{-1/3} \cdot T^{-1/2} \cdot N^{2/3} = f(C_W, C_{SiO_2}, N) \tag{8}$$

where f is a symbolic expression indicating a function of C_W, C_{SiO_2} and N. This equation allows us to estimate the decompression rate $|dP/dt|$ from the BND value N, when the H_2O and SiO_2 contents are given; it is referred to as the BND decompression rate meter.

Fig. 5(a) and (b) show the contour lines of decompression rates as functions of H_2O and SiO_2 contents for BNDs of 10^{11} and 10^{14} (m^{-3}), respectively. These figures present two important aspects. One is that the contour lines in these two figures take the same geometry because of the identical dependence on SiO_2 and H_2O contents and because the difference of three orders of magnitude in BND results in a difference by two orders of magnitude of the estimated decompression rate. Another is that the initial H_2O content does not exert a large influence (a maximum of 1.5–2 factors for a 4–8 wt.% H_2O content variation), whereas the SiO_2 content exerts a large influence (one order of magnitude for 50–75 wt.% SiO_2 content variation) on the estimated values of the decompression rates.

Fig. 6 shows the contour lines of the decompression rates as functions of log (N) and the SiO_2 content with H_2O content as a parameter. From this figure, it is observed that even if the H_2O content varies by ±2 wt.% from 6 wt.% the influence on the estimation of the decompression rates is minimal. In the case of eruptions with nearly identical N values, a decrease in SiO_2 contents implies an increase in the decompression rate whereas a decrease in N implies a decrease in the decompression rate for similar SiO_2 contents.

3. Application to Plinian eruptions

Since H_2O content does not significantly affect the estimation of the decompression rate for the relatively large H_2O contents that are expected in Plinian eruptions, we can assume a 5 wt.% H_2O content and estimate absolute values of the decompression rate for the 14 eruptions shown in Fig. 1. Fig. 7 shows the results with the correlation between the decompression rates obtained by the proposed method and the eruption column height data given by various methods (see Toramaru (1990) for historical eruptions of Towada and Izu-Oshima volcanoes, Holasek and Self (1995) for Mount St. Helens 1990 eruption, Holasek et al. (1996) for Mount Pinatubo 1990 eruption and Endo et al. (1988) for Izu-Oshima 1986 eruption) (see Table 1). From this figure, we observe that the estimated decompression rates range from 10^6 to 10^8 (Pa/s). These values are very high; thus, the existing models of conduit flows cannot explain them, as discussed in a later section.

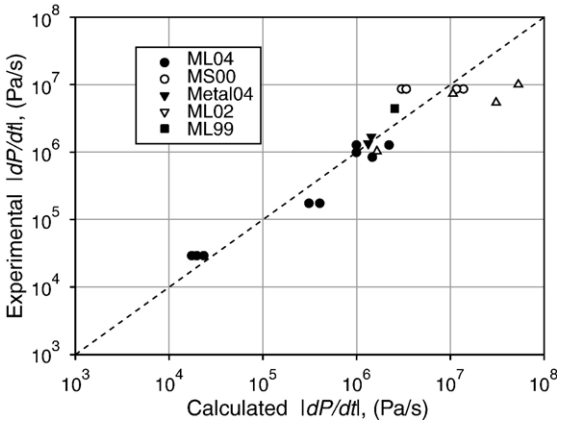

Fig. 4. Experimental decompression rates vs. calculated decompression rates obtained by using the decompression rate meter described in this paper.

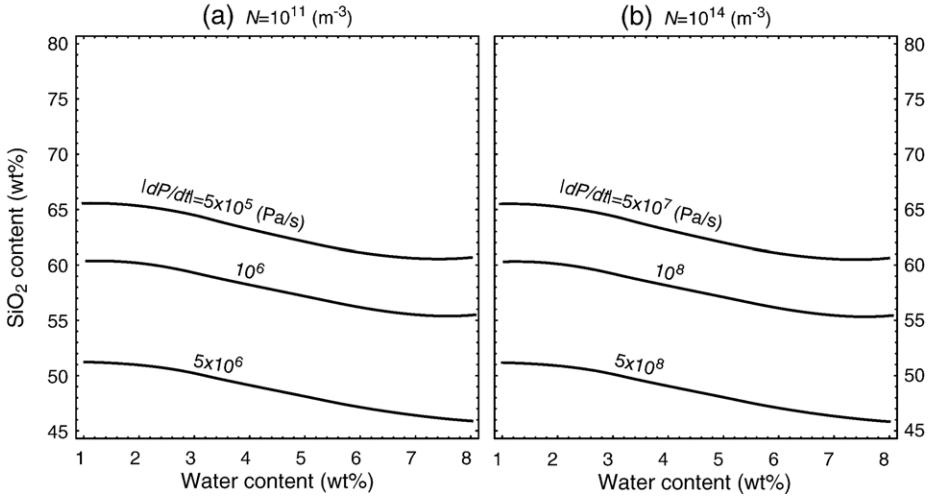

Fig. 5. Contour plots of the decompression rate as functions of SiO_2 contents and H_2O contents. (a) BND = 10^{11} (m^{-3}), (b) BND = 10^{14} (m^{-3}).

Another important aspect that is evident from this figure is the rough correlation between the decompression rates and eruption column heights H_T,

$$\left|\frac{dP}{dt}\right| \propto H_T^4. \tag{9}$$

This result is a new scaling relation that concerns the intensity of an explosive eruption; this relationship connects both an observable quantity on the surface, H_T and a quantity that represents the intra-conduit physics, $|dP/dt|$.

The column height in the Plinian eruption is proportional to one-fourth the discharge rate (Wilson et al., 1978) Q:

$$H_T \propto Q^{1/4}. \tag{10}$$

Thus, the decompression rate linearly correlates with the discharge rate:

$$\left|\frac{dP}{dt}\right| \propto Q. \tag{11}$$

These relationships inferred from the BND decompression rate meter might strongly constrain the mechanism

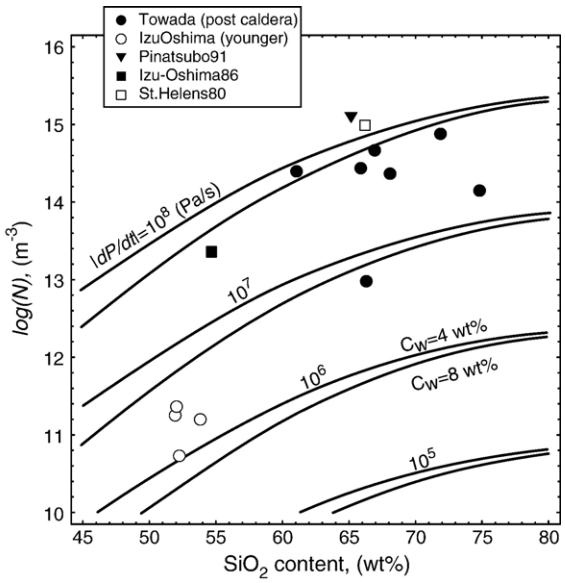

Fig. 6. LogBND (m^{-3}) vs. SiO_2 content (wt.%) for 14 Plinian to subplinian eruptions. Contours of decompression rate $|dP/dt|$ (Pa/s) with a water content parameter of 4 (upper bound) and 8 (lower bound) wt.% are also depicted.

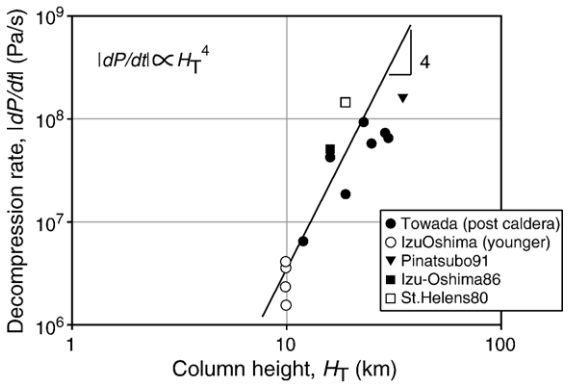

Fig. 7. Correlation between the decompression rates (Pa/s) estimated for the 14 eruptions mentioned in Fig. 1 and the eruption column height (km). A straight line indicates the proportionality between log ($|dP/dt|$) and column height with a slope of 4. The symbols are the same as in Fig. 1. The automatic regression line has a best-fit slope of 3.15 and $R^2=0.77$.

of explosive volcanic eruptions; hence, we discuss this in detail in the next section.

Since the discharge rate is proportional to the exit velocity for a constant conduit radius, it might be inferred that the decompression rates are proportional to the exit velocities. However, this is unlikely because the exit velocity cannot vary by two orders of magnitude.

4. Discussions

The two main points in the above results are as follows: 1) The estimated decompression rates ranging from 10^6 to 10^8 (Pa/s) are rather high. 2) There appears to be a linear relationship between the decompression rates and discharge rates. These two points are closely related to the manner in which decompression occurs in the conduit. In this section, we examine whether the existing model can explain these inferred facts and propose a possible model of vesiculation and decompression in the conduit.

4.1. Factors controlling decompression rate

The decompression rate estimated by the above method is a Lagrangian decompression rate, in other words, the decompression rate at a point moving together with ascending magma. In such a case, we can describe the decompression rate in terms of the pressure gradient, ascent velocity, and Eularian decompression rate:

$$\left(\frac{\mathrm{d}P}{\mathrm{d}t}\right)_{z_n} = \left(\frac{\partial P}{\partial z}\right)_{z_n} \cdot \left(\frac{\partial z}{\partial t}\right)_{z_n} + \left(\frac{\partial P}{\partial t}\right)_{z_n} \qquad (12-1)$$

$$= \left(\frac{\partial P}{\partial z}\right)_{z_n} \cdot \upsilon(z_n) + \left(\frac{\partial P}{\partial t}\right)_{z_n} \qquad (12-2)$$

where $(\partial P/\partial z)_{z_n}$ is a pressure gradient, $\upsilon(z_n)$ is the ascent velocity, and $(\partial P/\partial t)_{z_n}$ is the Eularian decompression rate; these three variables are considered with respect to the nucleation depth z_n. The first term of RHS is the steady state contribution to the decompression rate whereas the second term is the transient contribution. The pressure gradient for a steady state is controlled by the magma-static pressure gradient, inertial force, and wall friction and viscous force F according to the momentum conservation for the constant cross section of the conduit (Wilson et al., 1980) as follows:

$$\left(\frac{\partial P}{\partial z}\right)_{z_n} = -\rho \cdot g - \rho \cdot \upsilon \cdot \left(\frac{\partial \upsilon}{\partial z}\right)_{z_n} - F. \qquad (13)$$

In a simple uniform flow (simplest case), the second and third terms on the right-hand side of Eq. (13) can be neglected, and $\upsilon(z_n)=\upsilon_{exit}$ can be assumed. This corresponds to a pressure change due to the unloading of mass from a vent. In such a case, for $\upsilon_{exit}=10$ to 100 (m/s) and $\rho=1000$ (kg/m^3), the absolute values of the decompression rate are estimated in the range from 10^5 to 10^6 (Pa/s). These values are very small and thus cannot explain the decompression rates estimated by the BND decompression rate meter. In addition, the decompression rate linearly correlates with the exit velocity. Although this seems to be consistent with Eq. (11), it is evident that such a speculation is not realistic because the exit velocity cannot vary by two orders of magnitude in the Plinian eruptions.

In more realistic cases (e.g., Dobran, 1992), where the wall friction and inertia are considered, the pressure gradient is several times larger than the magma-static pressure gradient. The decompression rate then becomes several times larger than that in the simplest case; however, the values are still rather small and hence cannot explain the estimated values of the decompression rate.

In a more general case, the conduit cross section A can spatially vary along the conduit axis. In this case, the mass conservation equation is combined to solve the change in pressure and velocity (Wilson et al., 1980): the equation ($\rho\upsilon A=$const) can be reduced to

$$\left(\frac{\partial \upsilon}{\partial z}\right) = \frac{\upsilon}{A}\left(\frac{\partial A}{\partial z}\right) + \frac{M^2}{\rho\upsilon}\left(\frac{\partial P}{\partial z}\right),$$

where the density is taken into account as a function of pressure $\rho=\rho(P)$ and M is the Mach number. In an incompressible (bubble-free) magma with a constant cross section of the conduit, the velocity and pressure are determined by the overpressure at the magma chamber and Eq. (13), as mentioned above. On the other hand, a compressible (bubble-bearing) magma with a varying conduit cross section, the velocity and pressure

can be obtained by solving the mass and momentum conservation equations, given the conduit geometry, rather than the overpressure of magma chamber. In the present case, where bubbles do not exist in the magma (i.e., incompressible magma) before the bubble nucleation, the velocity gradient is related to the along-conduit variation of the cross section. It is possible that the pressure gradient associated with the conduit cross section variation produces a higher decompression rate, that is, the local narrowness of the conduit yields a local high velocity gradient. However, it appears that the conduit narrowness leads to an inverse correlation between the column height (the correlation with the discharge rate or erupted total mass is positive) and decompression rate. This is not the case. Therefore, we do not believe that such an external condition (conduit geometry) systematically controls the decompression rate in the conduit. Thus, it is concluded that existing conduit models cannot explain the estimated magnitude of decompression rates up to 10^8 (Pa/s).

One might think that the bubble nucleation near surface pressure (Legros and Kelfoun, 2000; Mastin et al., 2004) is related to a high decompression rate under a highly disequilibrium vesiculation process (Mangan et al., 2003). However, I believe that this is not the case because such a high decompression process can be possible in the case of the compressible (bubble-bearing) magma and because the pressure is ready to relax and cannot be maintained at a high pressure of the orders of 10^8 (Pa) as the magma reaches the near-surface condition. However, more studies are required to thoroughly examine whether such possibilities are realistic.

4.2. Bubble nucleation as a rarefaction shock wave: a proposal

In this section, we propose a new model for decompression and bubble nucleation processes in the conduit, which possibly explains the estimated magnitude of the decompression rate. First, we illustrate an important effect of bubble nucleation on the dynamics of conduit flow and show that bubble nucleation is accompanied by a shock wave, specifically, a rarefaction shock wave.

The bubble nucleation requires a non-zero value of supersaturation or over-pressure. This supersaturation has a significant influence on the history of volume change in vesiculating magmas, which controls the behavior of magma as a compressible fluid. For instance, the specific volume of magma suddenly increases at nucleation pressure as seen in the pressure-volume (P–V) curve (Fig. 8). Thus, the bubble nucleation creates a region with negative curvatures in a P–V curve, such that the second law of thermodynamics allows the presence of a rarefaction shock wave (see Appendixes for the details). On the other hand, ordinary materials, which are characterized by normal properties without any phase transformation during decompression, do not allow the stable propagation of a rarefaction shock wave. A compressible shock is possible in such ordinary materials, that is, a rarefaction or negative shock is ruled out.

If the bubble nucleation propagates into the conduit as a rarefaction shock wave, the decompression rate is controlled by the pressure difference ΔP, shock thickness Δz, and the propagation velocity Ω, as follows (Fig. 9):

$$\left|\frac{\mathrm{d}P}{\mathrm{d}t}\right| = \frac{\Delta P}{\Delta z}\cdot\Omega = \frac{\Delta P}{\Delta t} \tag{14}$$

where Δt is the travel time through the shock $\Delta z/\Omega$. It is probable that the decompression rate controlled by the rarefaction shock takes values up to 10^8 (Pa/s) orders of magnitude since the pressure difference is 10^7 (Pa/s) orders of magnitude (Mourtada-Bonnefoi and Laporte, 2002, 2004; Mastin et al., 2004; Mangan and Sisson, 2005), and the propagation velocity is 100 (m/s) orders of magnitude, assuming $\Delta z = 10$ (m). In the following paragraphs and Appendixes, we discuss these values in greater detail.

On the basis of the principle of conservation of mass and momentum (see Appendixes), we obtain the following equations for the velocity of discontinuity Ω and the downstream velocity U_2.

$$\Omega = V_1\left(\frac{\Delta P}{\Delta V}\right)^{\frac{1}{2}} \tag{15}$$

$$U_2 = (\Delta P\cdot\Delta V)^{\frac{1}{2}} \tag{16}$$

where $\Delta V = 1/\rho_2 - 1/\rho_1 = V_2 - V_1$ and $\Delta P = P_1 - P_2$. The above expression for shock velocity is fundamentally identical to Hill's result (Hill, 1991) for an evaporation wave, although he used the energy equation to relate the volume difference of $V_2 - V_1$ to the Jacob number (ratio of latent heat to superheat), which determines the volume fraction of a gas phase in a two-phase region.

Assuming that the entropy production accompanied with the propagation of a shock wave is very small, the isentrope ($P-V$ curve) is equivalent to the Hugoniot curve. The Chapman–Jouguet shock condition is also assumed to be satisfied. These assumptions imply that the propagation velocity equals the sound speed of the two-phase material in the downstream low-pressure region. If the surface tension is 0.1 (N/m) and the initial saturation pressure P_0 is 200 (MPa), $\Delta P \approx 0.1\times 200\times 10^6$ (Pa) and $\Delta V \approx 0.1\times 1/\rho$ (m^3) (see Fig. 8), where ρ represents the

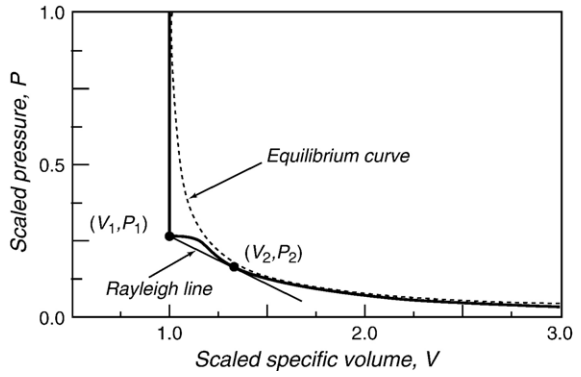

Fig. 8. Pressure–volume curve (P–V) curve (thick solid line) for a magma with bubble nucleation. The pressure is scaled by the initial saturation pressure P_0. The volume is scaled by the specific volume of the magma before bubble nucleation or $V_0=1/\rho$ (m^3/kg). The dashed line is the equilibrium P–V curve. The thin straight line is the "Rayleigh line", which controls the propagation velocity of the shock wave. An initial saturation pressure of 200 (MPa) and surface tension of 0.1 (N/m) are assumed to calculate the $P-V$ curve using the vesiculation model (Toramaru, 1995).

density of silicate melts (=2500). These values yield $\Omega\approx(1/2500)\times(200\times10^6\times2500)^{1/2}\approx300$ (m/s) and $U_2\approx0.1\times(200\times10^6/2500)^{1/2}\approx30$ (m/s). If $\Delta z\approx10$ (m) (see Appendixes), from Eq. (13), $|dP/dt|\approx2\times10^7\times300/10\approx5\times10^8$ (Pa/s). Thus, a rarefaction shock wave accompanying bubble nucleation can generate a high decompression rate, as inferred from the BND decompression rate meter.

Next, in order to examine the relationship expressed in Eq. (11) we consider the types of parameters that control both $|dP/dt|$ and Q, values of which vary by two orders of magnitude. On the basis of the abovementioned argument, $|dP/dt|$ is given by $\Delta P\cdot\Omega/\Delta z$. ΔP is approximated by the nucleation pressure P_n (pressure at which the nucleation rate achieves the maximum value), which is proportional to the initial saturation pressure P_0 with a factor of the order of 0.1, $\Delta P\approx O(0.1)\cdot P_0$. $\Delta V=\Delta C_{H_2O}\cdot R\cdot T\times(1/\rho)$, assuming an ideal gas for the exsolved H_2O, where R is the gas constant. The concentration difference ΔC_{H_2O} (mol/m^3) between the regions before and after the shock is given by $C_{H_2O}(P_0)-C_{H_2O}(P_n)\approx k_s\cdot P_0^{1/2}\cdot[1-(P_n/P_0)^{1/2}]\approx O(0.1)\cdot k_s\cdot P_0^{1/2}$, where k_s is the solubility constant (=0.58) and $1-((P_n/P_0)^{1/2}=\text{const.}=O(0.1)$. Hence, $\Delta V=O(0.1)\times k_s\cdot P_0^{-1/2}\cdot R\cdot T\cdot\rho^{-1}$ and $\Omega=P_0^{3/4}\cdot(k_s\cdot R\cdot T\cdot\rho)^{-1/2}$. As a result, we obtain the decompression rate as a function of initial saturation pressure, solubility constant, temperature, and shock thickness:

$$\left|\frac{dP}{dt}\right|\approx O(0.1)\times(k_s\cdot R\cdot T\cdot\rho\cdot\Delta z^2)^{\frac{1}{2}}\times P_0^{\frac{7}{4}}. \quad (17)$$

Thus, the decompression rate is approximately proportional to the square of the initial saturation pressure, provided that Δz is constant (constant shock thickness hypothesis). Since P_0 is proportional to the square of the initial H_2O content C_W, the decompression rate strongly depends on the 4th power of C_W. If the initial H_2O content of two magmas differ by a factor of 3 (e.g., 2 and 6 wt.%), then resulting decompression rates vary by two orders of magnitude.

With regard to Q, Carey and Sigurdsson (1989) encountered a similar problem. They argued that the variation of Q by two orders of magnitude is caused by an interplay of the ascent velocity, conduit erosion,

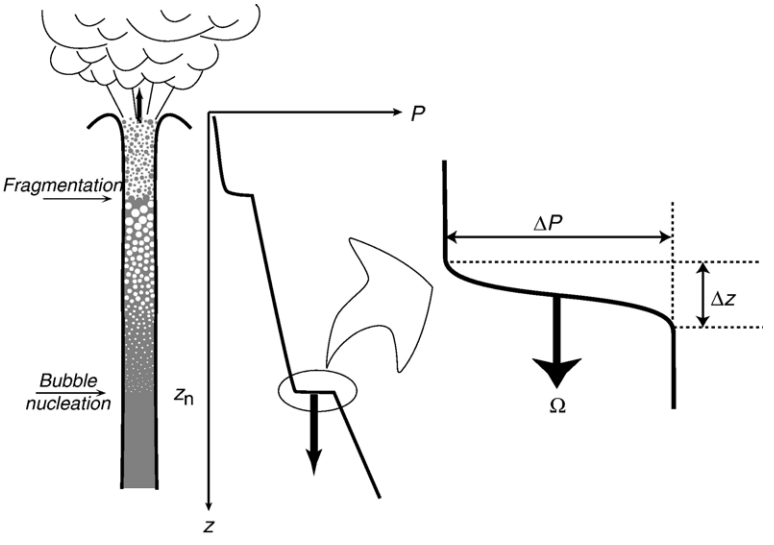

Fig. 9. A schematic figure showing the relationship between the rarefaction shock propagation and the decompression rate.

erupted total mass, and eruption duration. Additionally, it is likely that the total erupted mass and eruption duration correlate with the SiO_2 content and initial H_2O content because larger magmatism is more silicic and includes more water (Smith, 1979). As a result, the variation in the initial water content by a factor of three amplifies the variation in the discharge rate by two orders of magnitude by the interplay of the water content, ascent velocity, conduit erosion, erupted total mass, and eruption duration. Although it is difficult to express this relationship by using a simple mathematical formula, it is inferred that the discharge rate is proportional to the square of the initial saturation pressure, i.e., $Q \propto P_0^2$. Hence, this equation along with Eq. (17) results in Eq. (11).

Despite various ambiguities, the above argument seems to account for the inferred magnitudes of the decompression rates as well as the inferred correlation between the decompression and discharge rates. Hence, I believe that the rarefaction shock model needs to be examined in greater detail as a new aspect of the conduit process. In conclusion, the inferred correlation between $|dP/dt|$ and Q Eq. (11) shows the variation in the H_2O content of magmas through the control on both $|dP/dt|$ and Q.

Finally, I would like to comment on the implication of the rarefaction shock model for the fragmentation mechanism. The steep pressure change through a rarefaction shock wave is accompanied by the abrupt expansion of the magma. Such an abrupt change in pressure and volume due to a rarefaction shock causes a fragmentation of the magma.

4.3. Uncertainty in the BND decompression rate meter

Recently, Yamada et al. (2005) presented a rigorous theory on bubble nucleation by using the analytical formula of the BND. Their result and that by Toramaru (1995) show almost the same dependence of BND on the decompression rate and physical properties such as diffusivity and surface tension. This agreement implies that the present model as the basis of the BND decompression rate meter is correct with regard to the parameter dependence. The only difference is the factor that is less than 10 (Yamada et al., 2005). In the present model for the BND decompression rate meter, this influences the factor a_0 of Eq. (2). In the present paper, in order to resolve this discrepancy, we introduced the adjustable constant a in Eq. (8), which is $3 \times a_0$, to best explain the experimental BND data.

In the present paper, Eq. (3) was transformed to the function of H_2O content by using the solubility relation. In this case, the effect of the H_2O content on interfacial tension is taken into account to a reasonable extent, including the change in H_2O content with progressive vesiculation. However, bubble nucleation happens as the single event with the initial H_2O content because a condition of no pre-existing bubbles and no gas release is assumed. Therefore, we can use the initial saturation pressure corresponding to the initial H_2O content to estimate the interfacial tension at the nucleation event. Bagdassarov et al. (2000) also provide the values of $d\sigma/dC_W$. The comparison of Eq. (6) and a linear relation that assumes the constant $d\sigma/dC_W(-20$ mN/m/wt.%) is given in Fig. 10. From this figure it is evident that the dependence of interfacial tension on the H_2O content is similar in both relations. Calculated values of interfacial tension that are systematically lower than the measured values may imply some systematic errors in the estimation of the decompression rates; however, this is not the case. Such ambiguity in the absolute values of the interfacial tension is accounted for by the adjustable constant, a. As a is determined by fitting the experimental values of the BND to a given decompression rate, the ambiguity in the absolute value of the interfacial tension does not affect the results of the present paper. On the other hand, the dependence of interfacial tension on the H_2O content is an important factor. The systematic discrepancy between the calculated values and measured ones (values calculated using Eq. (3) are lower than those obtained by experiments) as functions of the H_2O content (Fig. 10) is due to the anomalously enriched water in melt drops for given gas pressure, e.g., experimental data (Table 3 in Bagdassarov et al. (2000)) show a value of 7.2 wt.% at 1 kbar; however, normally the solubility of water at 1 kbar is approximately 4 wt.%. In addition it is still uncertain whether the decrease of gas/melt interfacial tension with pressure is due to the effect of the dissolved H_2O content (the effect of water molecules in the melt phase) or the gas phase (water-saturated) pressure (the effect of water pressure in the gas phase). However, this uncertainty does not result in any significant error in the estimation of the decompression rate by the BND decompression rate meter, as explained above.

Mangan and Sisson (2005) estimated the surface tensions of the water/melt interface on the basis of the fact that the critical supersaturation pressure for nucleation depends only on the surface tension (Toramaru, 1995; Yamada et al., 2005): they argued that the surface tension strongly depends on the SiO_2 content or the fractionation index. However, given the experimental decompression rates, the BNDs estimated using their estimated surface tension data are not consistent with the actual experimental BNDs. For instance, in dacite experiments by Mangan and Sisson (2005) the calculated BNDs (m^3) are

6.8×10^{10}, 1.8×10^{10}, and 7.0×10^{9}, and the experimental maximum BNDs are 1.1×10^{12}, 1.3×10^{12}, and 3.5×10^{12} for the conditions (T (°C), C_W (wt.%), σ(N/m))=((950, 5.7, 0.04), (1000, 5.2, 0.06) and (1055, 4.8, 0.073), respectively, assuming a decompression rate of 2 MPa/s. Hence, we need to study the nature of surface tension in greater detail since the SiO_2 content influences the geometry of the contour lines shown in Fig. 5. Consequently, in the present BND decompression rate meter, we do not consider the SiO_2 dependence of surface tension. A further improvement of the BND decompression rate meter is highly desired along with a precise determination of the dependence of surface tension on H_2O and SiO_2 contents by experiments.

4.4. Important points to consider when using the BND decompression rate meter

There exists a crucial aspect to be considered when using the BND decompression rate meter. First, we have to carefully choose pumice or scoria samples that definitely preserve the history of homogeneous nucleation. A possible criterion is a bubble size distribution with a narrow size range similar to an exponential distribution (Toramaru, 1989; Blower et al., 2002) because a power-law type distribution with a wide spectrum shows a high possibility of the occurrence of heterogeneous nucleation, bubble coalescence, or Ostwald ripening occurs (Mangan and Cashman, 1996; Gaonac'h et al., 1996; Blower et al., 2002). Although there is a possibility that a few images of vesicle texture used in the present study do not exactly satisfy this criterion (Blower et al., 2002), the main trend of the correlation will not change significantly.

Recently Massol and Koyaguchi (2005) showed that a second nucleation event may occur under an accelerating $|dP/dt|$ condition induced by the magma ascent for certain parameter ranges, even if the homogeneous nucleation is assumed. This complex phenomenon must be considered in future interpretations of the vesicle texture. However, at present, in the absence of an established criterion for the discrimination of the second nucleation, the analysis of this phenomenon is of no consequence.

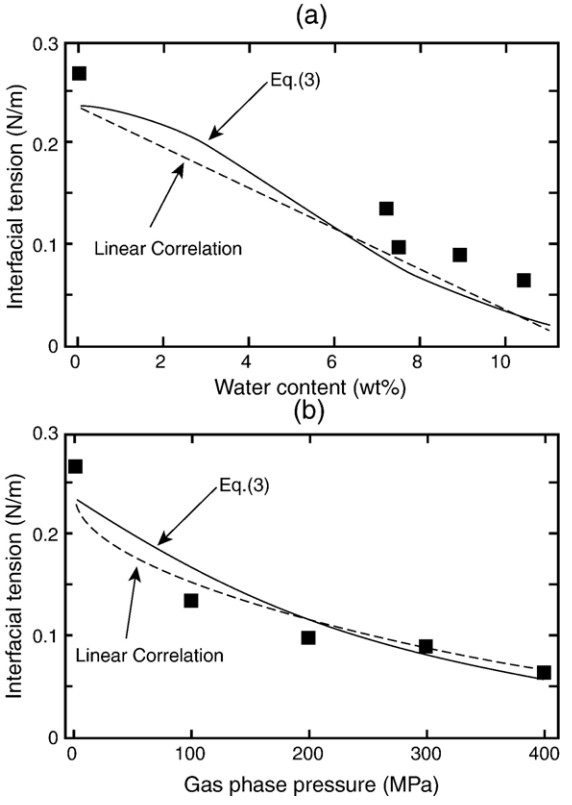

Fig. 10. Interfacial tension vs. water content (a) and gas phase pressure (b). Solid curves represent the Eq. (3). Dashed curves represent the linear relation between the interfacial tension and the water content as the control point for zero water content. Data points from Bagdassarov et al. (2000).

5. Conclusions

We created the BND decompression rate meter with regard to Plinian eruptions. The BND decompression rate meter is applicable to eruptions that are characterized by the occurrence of a single homogeneous nucleation event. By applying the BND decompression rate meter to 14 eruptions, we found that the decompression rates are correlated with the eruption column heights and inferred that they are proportional to the discharge rates. This relation is possibly explained by a new model of conduit flow in which bubble nucleation along with a rarefaction shock wave propagates into the conduit. This work is an attempt to construct a method (BND decompression rate meter) for erupted products, although it is clear that this method requires improvement and a higher degree of sophistication in the future with regard to its usage and construction.

Acknowledgments

The author thanks T. Miwa for the discussion and textural observation of pumice samples. He also thanks Margaret Mangan, Larry Mastin, and an anonymous reviewer for their helpful and constructive comments. This work was partially supported by a Grant-in-Aid for Scientific Research from MEXT (No. 14080202 and No. 17340131).

Appendix A. Brief argument on the thermodynamics and fluid mechanics of a rarefaction shock wave

A rigorous argument can be made on the basis of thermodynamics. Let us consider a system consisting of two fluids that are separated by a discontinuity (Fig. 11). The entropy change of the fluid flow from a high-pressure region to a low-pressure region through the discontinuity S_2-S_1 is given by the following equation (Landau and Lifshitz, 1959; Zeldovich and Raizer, 1967)

$$S_2-S_1=\frac{1}{12T_1}\left(\frac{\partial^2 V}{\partial P^2}\right)_S(P_2-P_1)^3 \qquad (A-1)$$

where T is the temperature; V, the specific volume; and P, the pressure. A single-phase material usually has a positive value for the second derivative of the specific volume with respect to pressure for any pressure range. In other words,

$$\left(\frac{\partial^2 V}{\partial P^2}\right)_S>0. \qquad (A-2)$$

As a result, in order to satisfy the second law of thermodynamics (i.e., $S_2-S_1>0$), $P_2>P_1$ is required. This implies that a discontinuity can be formed in the compression wave but not in the expansion (rarefaction) wave in ordinary materials.

On the other hand, in systems wherein a first order phase transformation such as vesiculation occurs, the P–V curve takes the negative value of the second derivative. Namely the negative curvature in the P–V curve due to the kinetic effect, as explained in the text.

$$\left(\frac{\partial^2 V}{\partial P^2}\right)_S<0 \qquad (A-3)$$

If the second derivative takes a negative value, the second law of thermo-dynamics allows the condition for $P_1>P_2$. This means that a rarefaction shock can exist in such a system (Zeldovich and Raizer, 1967; Thompson and Lambrakis, 1973; Borisov et al., 1983; Thompson et al., 1986).

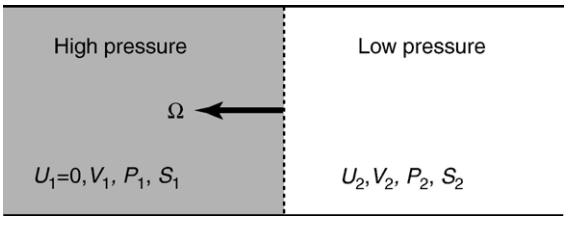

Fig. 11. A system comprising two fluids that are separated by a discontinuity (dashed line).

If the discontinuity exists, we can consider the conservation of mass, momentum, and energy together through the discontinuity and can use the normal method to obtain flow properties such as the velocity of discontinuity Ω and two-phase mixture velocity in a low pressure region U_2:

(a) mass conservation:

$$\rho_1\Omega=\rho_2(\Omega-U_2) \qquad (A-4)$$

(b) momentum conservation:

$$P_1+\rho_1\Omega^2=P_2+\rho_2(\Omega-U_2)^2 \qquad (A-5)$$

(c) energy conservation:

$$H_1+\frac{1}{2}\Omega^2=H_2+\frac{1}{2}(\Omega-U_2)^2 \qquad (A-6)$$

where ρ is density ($=1/V$) and H is the enthalpy, and subscripts 1 and 2 denote regions 1 and 2, respectively. Eqs. (15) and (16) can be obtained from Eqs. (A-4) and (A-5).

Appendix B. Evaluation of shock thickness

It is difficult to evaluate the shock thickness Δz and the travel time (relaxation time) Δt due to an unknown interaction between the bubble formation kinetics and pressure relaxation. In this case, we make a rough estimation assuming that the travel time through the shock is equivalent to the relaxation time of the diffusive bubble growth, that is, $\Delta t=l^2/D$, where D is the diffusivity of water in the melts and l is a length scale characterizing the relaxation of supersaturation by diffusive bubble growth. The minimum estimation of the scale length is the critical bubble radius at the nucleation stage $l_{\min}=R_0=2\sigma/P_0$, which is of the order of 10^{-9} (m). On the other hand, the maximum estimation is the spacing between the bubbles, $l_{\max}=N^{-1/3}$, which is of the order of 10^{-4} to 10^{-5} (m) for a typical number densities of the order of 10^{12} to 10^{15} (m^{-3}). Hence, Δt has a range of $10^{-7}\ll\Delta t\ll10^{3}$ (s) for a typical value of D (10^{-11}) (m^2/s) As a result, we have a large range, $10^{-5}\ll\Delta z\ll10^{3}$ (m), for the shock thickness. The exact values depend on the manner as well as the time for which the disequilibrium is maintained during bubble nucleation and growth processes. The disequilibrium processes are still under study (Gardner et al., 2000; Mangan and Sisson, 2000): hence, we adopt $\Delta z\approx10$ (m) as a plausible value which is a constant (constant shock thickness hypothesis). The argument in this section is

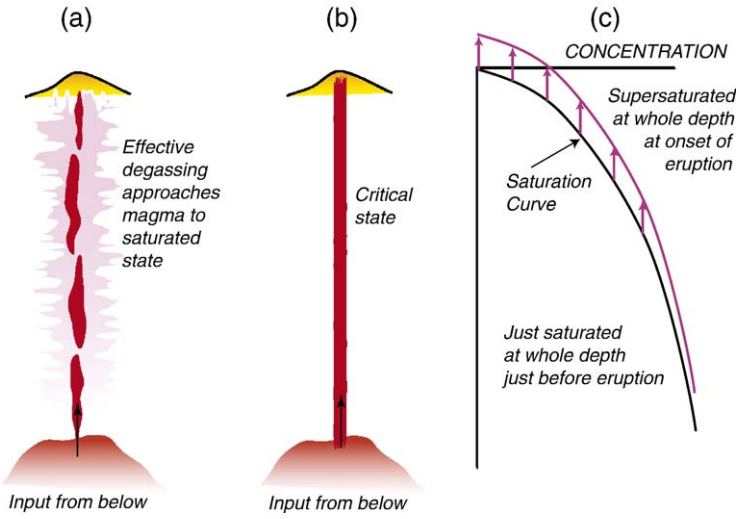

Fig. 12. Schematic figures showing the geologic situation in which the supersaturation occurs simultaneously throughout the conduit. (a) The early stage of pre-eruptive plumbing system. (b) The latest stage of pre-eruptive plumbing system. (c) The magma is saturated for the water with the solubility at the hydrostatic pressure throughout its depth just before the eruption. Then, the magma becomes supersaturated simultaneously throughout its depth at the onset of eruption (c).

very speculative; thus, more rigorous studies are required in the future.

Appendix C. Geological situation appropriate for the rarefaction shock model

The following is a brief summary of a geological situation in which the propagation of a rarefaction shock wave is analogous between a simple (Fig. 11) and a realistic (Fig. 12) volcanic system. The magma present in cracks or magma pockets rises at a relatively low velocity along or through a future conduit, exsolving and degassing the volatile components (Fig. 12 (a)). Eventually, individual bodies of rising magma combine or fill up the entire conduit. The magma filling the conduit flows at a relatively high velocity by the poiseuille-type flow, thereby limiting the extent of degassing (Fig. 12(b)). The overflow from the vent and the further upward migration of magma induce an over-saturated state throughout its depth; this triggers the vesiculation (Fig. 12(c)) (e.g., Mader et al., 1997). Thus it can be reasonably assumed that the initial volatile concentration in a conduit prior to eruption is distributed in equilibrium with the local hydrostatic pressure. In addition, the situation in which the magma is supersaturated throughout its depth is analogous to a geometrically simple superheated flow (Fig. 11). We can consider the propagation process in a stagnant magma column if the timescale of the rarefaction shock wave propagation is sufficiently shorter than that of the magma ascent.

References

Bagdassarov, N., Dorfman, A., Dingwell, D., 2000. Effect of alkalis, phosphorus, and water on the surface tension of haplogranite melt. Am. Mineral. 85, 33–40.

Behrens, H., Zhang, Y., Xu, Z., 2004. H_2O diffusion in dacitic and andesitic melts. Geochim. Cosmochim. Acta 68, 5139–5150.

Blower, J.D., Keating, J.P., Mader, H.M., Phillips, J.C., 2002. The evolution of bubble size distributions in volcanic eruptions. J. Volcanol. Geotherm. Res. 20, 1–23.

Burnham, C.W., 1975. Water and magmas; a mixing model. Geochim. Cosmochim. Acta 39, 1077–1084.

Borisov, A.A., Borisov, Al.A., Kutateladze, S.S., Nakoryakov, V.E., 1983. Rarefaction shock wave near the critical liquid-vapor point. J. Fluid Mech. 126, 59–73.

Carey, S., Sigurdsson, H., 1989. The intensity of Plinian eruptions. Bull. Volcanol. 51, 28–40.

Dobran, F., 1992. Nonequilibrium flow in volcanic conduits and application to the eruptions of Mt. St. Helens on May 18, 1980, and Vesuvius in AD 79. J. Volcanol. Geotherm. Res. 49, 285–311.

Endo, K., Chiba, T., Taniguchi, Sumita, M., Tachikawa, S., Miyahara, T., Uno, R., Miyaji, N., 1988. Tephrochronological study on the 1986–1987 eruptions of Izu-Oshima volcano, Japan. Bull. Volcanol. Soc. Jpn. 33, S32–S51.

Gaonac'h, H., Lovejoy, S., Stix, J., Schertzer, D., 1996. A scaling growth model for bubbles in basaltic lava flows. Earth Planet. Sci. Lett. 139, 395–409.

Gardner, J.E., Denis, M.-H., 2004. Heterogeneous bubble nucleation on Fe–Ti oxide crystals in high-silica rhyolitic melts. Geochim. Cosmochim. Acta 68, 3587–3597.

Gardner, J.E., Thomas, R.M.E., Jaupart, C., Tait, S., 1996. Fragmentation of magma during Plinian volcanic eruptions. Bull. Volcanol. 58, 144–162.

Gardner, J.E., Hilton, M., Carroll, M.R., 1999. Experimental constraints on degassing of magma: isothermal bubble growth during continuous decompression from high pressure. Earth Planet. Sci. Lett. 168, 201–218.

Gardner, J.E., Hilton, M., Carroll, M.R., 2000. Bubble growth in highly viscous silicate melts during continuous decompression from high pressure. Geochim. Cosmochim. Acta 64, 1473–1483.

Hill, L.G., 1991. An experimental study of evaporation waves in a superheated liquid. Ph.D. dissertation, 184 pp, California Institute of Technology.

Holasek, R.E., Self, S., 1995. GOES weather satellite observations and measurements of the May 18, 1980 Mount St. Helens eruption. J. Geophys. Res. 100, 8469–8487.

Holasek, R.E., Self, S., Woods, A.W., 1996. Satellite observations and interpretation of the 1991 Mount Pinatubo eruption plumes. J. Geophys. Res. 101, 27635–27655.

Hurwitz, S., Navon, O., 1994. Bubble nucleation in rhyolitic melts: experiments at high pressure, temperature and water content. Earth Planet. Sci. Lett. 122, 267–280.

Jaupart, C., Allègre, C.J., 1991. Gas content, eruption rate and instabilities of eruption regime in silicic volcanoes. Earth Planet. Sci. Lett. 102, 413–429.

Klug, C., Cashman, K.V., 1994. Vesiculation of May 18, 1980, Mount St. Helens magma. Geology 22, 468–472.

Landau, L.D., Lifshitz, E.M., 1959. Fluid Mechanics. Pergamon, New York.

Larsen, J.F., Gardner, J.E., 2004. Experimental study of water degassing from phonolite melts: implications for volatile oversaturation during magmatic ascent. J. Volcanol. Geotherm. Res. 134, 109–124.

Legros, F., Kelfoun, K., 2000. Sustained blasts during large volcanic eruptions. Geology 28, 895–898.

Mader, H.M., Brodsky, E.E., Howard, D., Sturtevant, B., 1997. Laboratory simulations of sustained volcanic eruptions. Nature 388, 462–464.

Mangan, M.T., Cashman, K.V., 1996. The structure of basaltic scoria and reticulate and inferences for vesiculation, foam formation, and fragmentation in lava fountains. J. Volcanol. Geotherm. Res. 73, 1–18.

Mangan, M.T., Sisson, T.W., 2000. Delayed, disequilibrium degassing in rhyolite magma. Decompression experiments and implications for explosive volcanism. Earth Planet. Sci. Lett. 183, 441–455.

Mangan, M.T., Sisson, T.W., 2005. Evolution of melt-vapor surface tension in silicic volcanic systems: experiments with hydrous melts. J. Geophys. Res. 110, B01202. doi:10.1029/2004JB003215.

Mangan, M., Mastin, L., Sisson, T., 2003. Gas evolution in eruptive conduits: combining insights from high temperature and pressure decompression experiments with steady-state flow modeling. J. Volcanol. Geotherm. Res. 129, 23–36.

Mangan, M.T., Sisson, T.W., Hankins, W.B., 2004. Decompression experiments identify kinetic controls on explosive silicic eruptions. Geophys. Res. Lett. 31, L08605. doi:10.1029/2004GL019509.

Massol, H., Koyaguchi, T., 2005. The effect of magma flow on nucleation of gas bubbles in a volcanic conduit. J. Volcanol. Geotherm. Res. 143, 69–88.

Mastin, L.G., Christiansen, R.L., Thornber, C., Lowenstern, J., Beeson, M., 2004. What makes hydromagmatic eruptions violent? Some insights from the Keanakāko'i Ash, Kīlauea Volcano, Hawai'i. J. Volcanol. Geotherm. Res. 137, 15–31.

Mourtada-Bonnefoi, C.C., Laporte, D., 1999. Experimental study of homogeneous bubble nucleation in rhyolitic magmas. Geophys. Res. Lett. 26, 3505–3508.

Mourtada-Bonnefoi, C.C., Laporte, D., 2002. Homogeneous bubble nucleation in rhyolitic magmas: an experimental study of the effect of H_2O and CO_2. J. Geophys. Res. 107, B4. doi:10.1029/2001JB00290.

Mourtada-Bonnefoi, C.C., Laporte, D., 2004. Kinetics of bubble nucleation in a rhyolitic melt: an experimental study of the effect of ascent rate. Earth Planet. Sci. Lett. 218, 521–537.

Polacci, M., Papale, P., Rosi, M., 2001. Textural heterogeneities in pumices from the climactic eruption of Mount Pinatubo, 15 June 1991, and implications for magma ascent dynamics. Bull. Volcanol. 63, 83–97. doi:10.1007/s004450000123.

Proussevitch, A.A., Sahagian, D.L., 1996. Dynamics of coupled diffusive and compressive bubble growth in magmatic systems. J. Geophys. Res. 101, 17447–17455.

Smith, R.L., 1979. Ash-flow magmatism. In: Chapin, C.E., Elston, W.E. (Eds.), Ash-Flow Tuffs. Geol. Soc. Amer. Special Paper, vol. 180, pp. 5–27.

Sparks, R.S.J., 1978. The dynamics of bubble formation and growth in magmas: a review and analysis. J. Volcanol. Geotherm. Res. 3, 1–37.

Thompson, P.A., Lambrakis, K., 1973. Negative shock waves. J. Fluid Mech. 60, 187–208.

Thompson, P.A., Carofano, G.C., Kim, Y.-G., 1986. Shock waves and phase changes in a large-heat-capacity fluid emerging from a tube. J. Fluid Mech. 166, 57–92.

Toramaru, A., 1989. Vesiculation process and bubble size distributions in ascending magmas with constant velocities. J. Geophys. Res. 94, 17523–17542.

Toramaru, A., 1990. Measurement of bubble size distributions in vesiculated rocks with implications for quantitative estimation of eruption process. J. Volcanol. Geotherm. Res. 43, 71–90.

Toramaru, A., 1995. Numerical study of nucleation and growth of bubbles in viscous magmas. J. Geophys. Res. 100, 1913–1931.

Wilson, L., Sparks, R.S.J., Huang, T.C., Watkins, N.D., 1978. The control of volcanic eruption column heights by eruption energetics and dynamics. J. Geophys. Res. 83, 1829–1836.

Wilson, L., Sparks, R.S.J., Walker, G.P.L., 1980. Explosive volcanic eruptions. IV. The control of magma properties and conduit geometry on eruption column behavior. Geophys. J. R. Astron. Soc. 63, 117–148.

Woods, A.W., 1995. The dynamics of explosive volcanic eruptions. Rev. Geophys. 33, 495–530.

Yamada, K., Tanaka, H., Nakazawa, K., Emori, H., 2005. A new theory of bubble formation in magma. J. Geophys. Res. 110, B02203. doi:10.1029/2004JB003113.

Zeldovich, Y.B., Raizer, Y.P., 1967. Physics of Shock Waves and High-Temperature Hydrodynamic Phenomena. Academic press, New York.

Zhang, Y., Behrens, H., 2000. H_2O diffusion in rhyolitic melts and glasses. Chem. Geol. 169, 243–262.